On Neural-Network Representation of Wireless Self-Interference for Inband Full-Duplex Systems

Gerald Enzner, Aleksej Chinaev
Department of Medical Physics and Acoustics
Carl von Ossietzky Universität Oldenburg
26111 Oldenburg, Germany
{gerald.enzner, aleksej.chinaev}@uni-oldenburg.de

Aydin Sezgin
Chair of Digital Communication Systems
Ruhr-Universität Bochum
44780 Bochum, Germany
aydin.sezgin@ruhr-uni-bochum.de

***Abstract*—Nonlinear system modeling plays a pivotal role for interference cancellation in wireless systems with specifically high requirements of accuracy regarding the elimination of self-interference in full-duplex radios. The paper investigates the potential of identification and representation of the self-interference channel by neural network architectures. This digital approach is promising for its ability to cope with nonlinear representations, but the variability of channel characteristics would be an obstacle in straightforward application of data-driven neural networks. We hence propose architectures with adaptive elements to achieve successful training and testing. We document and share our data for reproducibility of results and for further investigations with possibly stronger models and enhanced performance.**

***Index Terms*—system modeling, neural networks, full-duplex**

I. Introduction

Inband full-duplex (IBFD) systems use one and the same frequency resource for simultaneous sending and receiving. Hence it requires cancellation of the strong self-interference (SI) of the transmitter into the receiver. The technology status implies possibilities of active or passive SI shielding in the propagation domain, adaptive or non-adaptive cancellation in the analog receiver unit, and adaptive cancellation in the digital baseband section of the receiver [1]–[3]. The different treatments would need to be joined to about 100 dB self-interference cancellation (SIC) in a system [4], [5]. Because of nonlinearity of the SI path, a fruitful link to predistortion technology in RF transmitters can be made also [6], [7].

The majority of approaches on the digital side has been concerned with signal processing for SIC using maximum-likelihood [8], subspace [9], mean-square error [10], least-squares [11], linear [12] and/or polynomial adaptive-filter methods [13], [14]. For relieving the extraordinary accuracy required for SIC, further approaches consists in the design of robust receivers via non-convex optimization [15] or modified matched filtering [16]. The transmitter side as well can be optimized to support the SIC task, e.g., by active injection of compensation signal [17] or by the choice of pilot sequences with favorable nonlinear behavior [18].

More recently, the SIC problem also has been approached with machine learning, specifically, with neural network representations [19]. Neural networks were shown to line up or even improve over linear and polynomial modeling accuracy, while reducing computational complexity [20]–[22]. Realtime assessment of neural networks was demonstrated in [23]. Frequently the SI modeling uses parallel linear and nonlinear components [22], [24], [25] and, more rarely, a cascaded representation [25] in a very interpretable fashion.

Ultimate utility of neural network models might be hampered by the fixed nature of trained models in case of time-varying SI channels and by the limited availability of datasets for comparative analysis and benchmarking of the models [19]. We note that the variability of SI channels is recently addressed in [25], [26]. Both of the aforementioned limitations are addressed with the approach of our paper. We specifically demonstrate the failure of common network architectures in case of variable linear or nonlinear elements in the data. As a remedy we therefore propose architectures which combine training and adaptation, i.e., with a subset of trainable weights to represent invariant and another subset of "adaptive" weights to fit variable characteristics of the data (not going as far as claiming online adjustment of the weights though). Moreover, the data prepared for our analysis is documented and made publicly available for reproducibility and further utilization in the community. The data is synthetic and meant as baseline for development and analysis, notwithstanding the utilization of real SI recordings which is beyond the scope here.

Sec. II depicts the full-duplex SI problem and two basic SIC options (named "Hammerstein" and "Wiener"). Sec. III describes our construction of research data with varying levels of difficulty. Sec. IV then introduces neural network architectures for the Hammerstein system option with different effort for coping with system variabilities. Sec. V presents results and comparison with baseline models, before Sec. VI concludes.

II. Overview of Full-Duplex System

From the wide range of possible SIC system options, we firstly consider the baseband design of Fig. 1.a. The transmit signal $s[k]$ at discrete time k is D/A converted and passed to the TX antenna via a nonlinear power amplifier (PA). The wireless SI path from the TX to the RX antenna is assumed to be linear. The parallel SIC path exhibits "Hammerstein" logic, i.e., nonlinearity $f(s)$ followed by a linear dynamical system w_k, to represent the PA and the linear SI path, respectively. The purpose of the parallel SIC path is to predict and cancel the SI $y_{\mathrm{H}}(t)$ in the analog domain before saturation of the low-noise amplifier (LNA) and the A/D converter in the receiver takes

This work is funded by the German Research Foundation (DFG) under Grant EN 869/4-1 with Project ID 449601577.

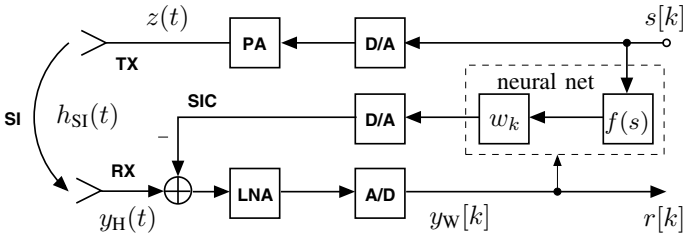

a) system option with "Hammerstein" network across D/A

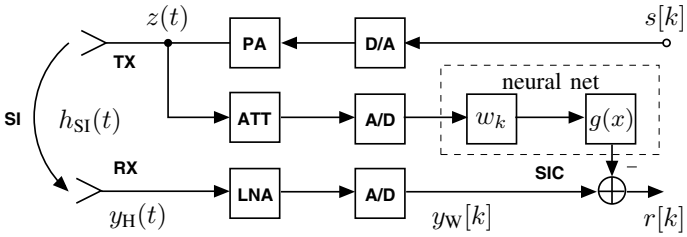

b) system option with "Wiener" type network across A/D

Fig. 1. System options with self-interference cancellation.

place. To this end, the network output passes through auxiliary D/A conversion and RF circuitry [27], [28]. The residual SI in the digital domain is termed $r[k]$. Other hardware impairments or the precise effect of the aforementioned RF circuitry will be neglected in our data. Our study is primarily concerned with simulation and treatment of SI path variabilities.

An opposite design may use "Wiener" logic, i.e., a linear dynamical model element w_k followed by nonlinearity $g(x)$ for SIC in Fig. 1.b. The transmit signal $z(t)$ after the power amplifier is captured by attenuation (ATT) circuitry to match the signal to the range of an auxiliary A/D converter. The conception here is that any PA nonlinearity is already encompassed by the utilization of the analog reference signal $z(t)$ as input for SIC and does not need to be modeled by the network [29], [30]. The inevitable saturation of the RX A/D is here addressed via the nonlinear element $g(x)$ to achieve SI modeling and subtraction from the received signal $y_{\rm W}[k]$.

III. Data Generation

For both system options of Fig. 1 we simulate high-throughput (HT) WLAN transmission [31] using orthogonal frequency-division multiplex (OFDM) signals in the complex baseband according to IEEE-802.11 [32], specifically, the n-channel with 20 MHz bandwidth and 64-QAM.

Our SI channel assumes separate antennas for up- and downlink with TX and RX at a distance of 30-50 cm [33]–[35]. The SI channel $h_{\rm SI}[k]$ simulated in the discrete-time domain is thus represented as a multipath model with two components: a dominant, quasi-static internal (or direct) path $h_{\rm iSI}[k]$ between TX/RX antennas and an external multipath $h_{\rm eSI}[k]$ due to reflections of the environment, i.e., $h_{\rm SI}[k] = h_{\rm iSI}[k] + h_{\rm eSI}[k]$. Furthermore, $h_{\rm SI}[k]$ is based on measurements in [35], where real SI channels of several environments were characterized such that (a) the power of the internal path is 5 to 10 dB higher than the strongest external path and (b) the root mean-square

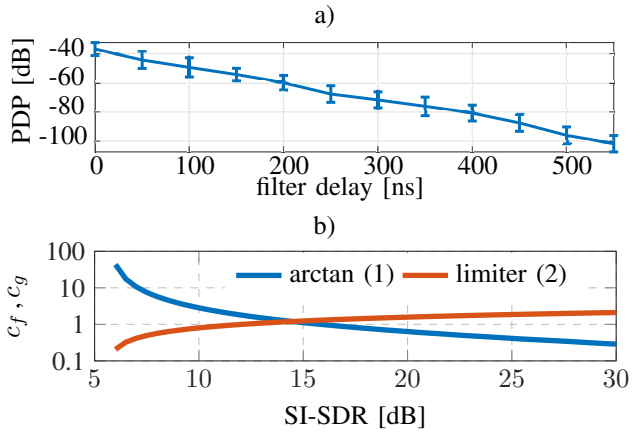

Fig. 2. Facts of the data generation: a) PDP of SI channels $h_{\rm SI}[k]$ with standard deviations; b) Parameters c_f and c_g vs. the SI-SDR.

(RMS) delay spread is in the range of 20 to 40 ns. Specifically, we rely on the WLAN multipath fading 'Model C' [31] and modify it[1] to meet these properties by our $h_{\rm SI}[k]$. The resulting power delay profile (PDP) is illustrated in Fig. 2.a and exhibits a duration of 550 ns (corresponding to 12 filter taps at 20 MHz sampling rate) to reach the noise floor.

The PA nonlinearity of Fig. 1 assumes only amplitude-to-amplitude (AM/AM) distortion [30], [37], while the receiver A/D is simulated as a saturation of its input signal, i.e.,

$$\mathrm{PA}(s) = F(|s|)\cdot e^{j\cdot\arg(s)}, \quad F(|s|) = f\cdot\arctan(c_f\cdot|s|) \quad (1)$$

$$\mathrm{AD}(y) = G(|y|)\cdot e^{j\cdot\arg(y)}, \quad G(|y|) = \begin{cases} |y|, & |y| < c_g \\ c_g, & |y| \geq c_g \end{cases}, \quad (2)$$

with unit-variance input s, the linear factor f to adjust the PA output to 20 dBm, and c_f and c_g as nonlinear scale and saturation parameters, respectively. The related distortions can be quantified by the scale-invariant signal-to-distortion ratio (SI-SDR) [38] as shown by Fig. 2.b.

The SIs in Fig. 1 are then simulated at discrete time k for the "Hammerstein" (H) system option as

$$y_{\rm H}[k] = \mathrm{PA}(\, s[k]\,) * h_{\rm SI}[k] + n[k] \quad (3)$$

and for the "Wiener" (W) system option as

$$y_{\rm W}[k] = \mathrm{AD}\big((\, z[k] * h_{\rm SI}[k] + n[k])\cdot\sqrt{10^5}\,\big), \quad (4)$$

where $*$ denotes discrete-time convolution, $n[k]$ is a receiver noise floor at -90 dBm/MHz, and we have 50 dB LNA gain.

Our datasets are constructed with variable or invariable SI channels and nonlinearities for both system options, labeled

(H) "invNL+invSI", "invNL+varSI", and "varNL+varSI"
(W) "invSI+invNL", "varSI+invNL", and "varSI+varNL",

each consisting of 10 files of simulated WLAN signals[2]. A variable SI channel per file is based on new path gains for $h_{\rm SI}[k]$, while variable nonlinearity is distributed uniformly in an 8 dB interval around mean SI-SDR$_0$ =10 dB.

[1]The Matlab WLAN Toolbox [36] is employed for implementation.

[2]The generated datasets and the MATLAB code for generation are available on GitHub under https://github.com/STHLabUOL/SICforIBFD. Larger datasets could be created for possibly large neural network models.

IV. Neural-Network Architectures

A range of models is presented to cope with the data according to the Hammerstein system of Fig. 1.a. The models are well guided by the Hammerstein configuration and implemented (including further baselines) with complex-valued computations for the complex baseband. The model sizes are deliberately small in terms of the number of trainable weights in order to support SI system identification with small amounts of data. The complex-valued residual $y_{\mathrm{H}}[k] - \widehat{y}_{\mathrm{H}}[k]$ between system and model is minimized via the MSE loss.

Fig. 3 shows a first model which is here termed "global" in the sense that a single set of trainable weights is optimized to fit all available "signals" (i.e., the files of a dataset) in the batch dimension of the input tensor. The temporal "samples" of each signal appear in the feature dimension. Cartesian $s[k]$ is firstly split into magnitude and phase to prepare for AM/AM nonlinear PA modeling [37], [39]. The actual nonlinearity of $f(s)$ in Fig. 1.a is here represented by a multilayer perceptron (MLP) with tanh activations, where the number of units P per hidden layer is implemented by filters of convolutional layers. A single output unit (linear) is then recombined with the original phase. The tensor format at this point of the model complies with the input tensor. In the final model stage, the temporal samples are taken to a complex-valued linear convolution with filter length L to represent the dynamical part w_k of the Hammerstein model.

The global Hammerstein representation is likely to fail when optimizing for datasets with variable SI channels $h_{\mathrm{SI}}(t)$ in different signals (i.e., file IDs). Our next model in Fig. 4 therefore retains the complex-valued MLP stage for nonlinear representation, but transposes the signals with possibly different SI channels to the last dimension of the tensor. A "depthwise" convolution (using Tensorflow jargon) can then apply its competence of individual kernels for individual signals in order to represent their individual SI channel. For its ability to host individual weights for each file ID, the model is here termed "adaptive". The output tensor of the convolution is finally reverse transposed to comply with the target signals for loss computation. The model bears functional similarity with the cascaded TID model in [25].

The last model in Fig. 5 applies a generalization of the nonlinear MLP stage while retaining the depthwise treatment and thus "adaptivity" of the previous model. Our nonlinear generalization adopts an architectural property of "parallel" Hammerstein modeling [40] by expanding the former single MLP output into P output units. This additional dimension enables the subsequent depthwise convolution to create individual nonlinear network behavior per file ID by forming different linear combinations from the P-dimensional MLP output. This effort goes with the hypothesis for successful modeling of both variable nonlinear and variable linear input-output relationship merely by means of linear parameters.

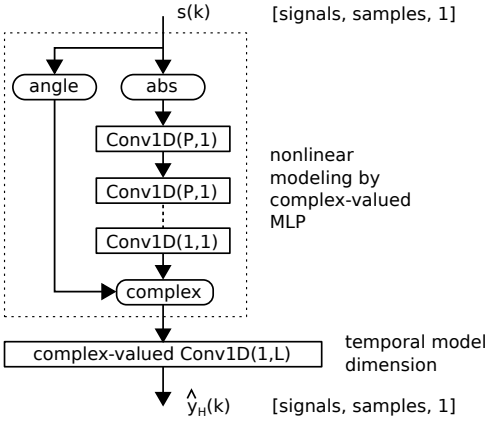

Fig. 3. Global complex-valued Hammerstein model.

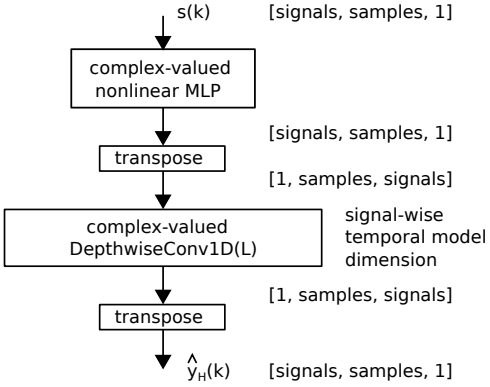

Fig. 4. Adaptive complex-valued Hammerstein model.

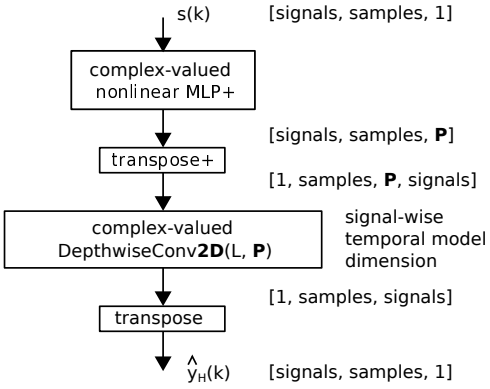

Fig. 5. Parallel adaptive complex-valued Hammerstein model.

V. Training and Evaluation

We here evaluate the Hammerstein subset of the data from Sec. III with various models. The Wiener data (while the data is provided) is not evaluated for space limitations in this paper. For the Hammerstein data our comparison includes

- the global Hammerstein model of Fig. 3
- the adaptive Hammerstein model of Fig. 4
- the parallel adaptive Hammerstein model of Fig. 5
- the time-delay feedforward neural network (FFNN) [22]
- the time-invariant nonlinear distortion (TID) model [25]
- and the memory polynomial (MP) model [13], [40].

The MLP of our Hammerstein models consists of 2 hidden layers with P=8 nonlinear units each, plus the output layer,

thus 8+64+8=80 trainable weights. The parallel Hammerstein model discards the output layer in order to provide P output units for nonlinear expansion. The linear convolution part of the global Hammerstein model uses kernelsize of L=32, thus over-modeling the 12 filter taps of our data construction. For adaptive Hammerstein modeling with 10 input files, the kernelsize multiplies to 10·32=320, and for parallel adaptive Hammerstein to 8·10·32=2560 trainable weights. It can be reported that straightforward upscaling of these model sizes would not deliver stronger results for the data at hand.

Our implementation of all models uses Tensorflow with the Keras backend. The following experiments use different subsets of data with increasing levels of difficulty by the data variability, i.e., "invNL+invSI", "invNL+varSI", and "varNL+varSI". All data files of one experiment together form a single batch for model optimization. Minimization of the MSE is pursued with a fixed number of 10^4 epochs in order to study the related learning behaviors. In all cases we rely on the Adam optimizer with learning rate of 0.01.

Fig. 6 firstly shows results for the invariant Hammerstein data ("invNL+invSI"). Model performances are compared in terms of overall SI attenuation $\mathrm{SIA} = \sigma_z^2/\sigma_{y_H-\widehat{y}_H}^2$, thus including the 35 dB passive SI isolation according to Fig. 2.a. A linear model on this nonlinear data is then limited to 50 dB, which is plausible with our SI-SDR of 10 dB of the data. The global Hammerstein model clearly better fits the nonlinear data and attains training SIA of about 85 dB. The model is validated to about the same SIA with test data constructed with different waveforms on the same nonlinearity and impulse response. The memory polynomial (MP) exhibits similar SIA. The FFNN network cannot fit the data at hand.

Fig. 7 steps up difficulty to SI data created with variable SI channels ("invNL+varSI"). Here, global Hammerstein modeling already fails to fit the training data, which is plausible from a perspective of nonlinear system identification on inconsistent plants (the global Hammerstein model supposedly represents an average of different SI channels). Our adaptive Hammerstein model with its individual kernel per training signal can fit the different SI channels and, hence, represent the inconsistent data. An SIA of 95 dB (notably a bit higher than in Fig. 6 before) is attained by the adaptive model with training and test data (the test data comprising of different waveforms, SI channels, and noise). To this end, the idea of "adaptivity" of the model extends into the test phase by adjusting the linear model part to the test data with few epochs. Under this circumstance, test performance even can be slightly higher than training performance of a model. The baseline MP degrades a little bit. The baseline TID aligns with adaptive Hammerstein. The FFNN baseline again falls behind.

Fig. 8 finally uses the data subset with variable SI channels and variable nonlinearities per signal ("varNL+varSI") which may further hamper system modeling by neural networks. The before successful adaptive Hammerstein model now indeed demonstrates an SIA limitation of 60 dB, but the parallel Hammerstein model in this case can restore 80 dB via its capacity of expanding the different nonlinear functions by individual

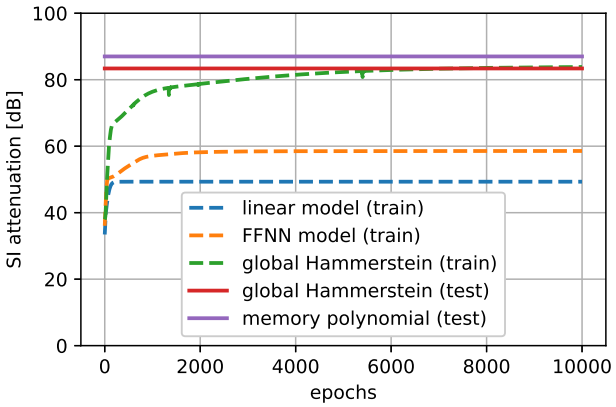

Fig. 6. Learning curve for the invariant Hammerstein SI data.

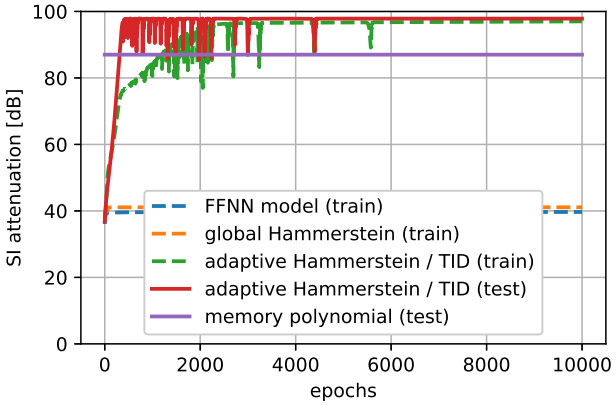

Fig. 7. Data with invariant nonlinearity and variable SI channel.

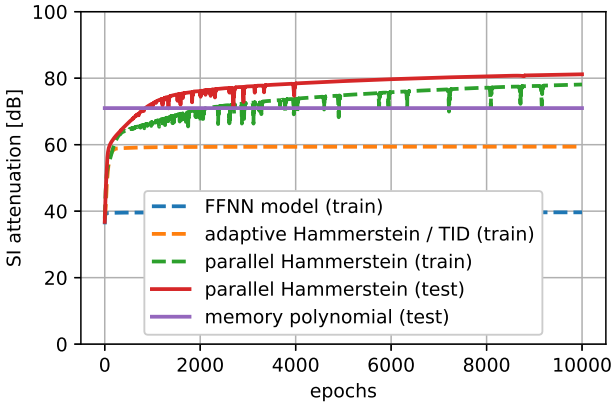

Fig. 8. Data with variable nonlinearity and variable SI channel.

kernels on the multiple MLP outputs. Once more, the required model "adaptivity" is implemented by adjusting all linear output weights to the test data. The average MP performance degrades to 70 dB with the variable nonlinearities, which can be traced to the signals with lowest SI-SDR in this dataset. Both the FFNN and TID baselines now fall behind.

VI. Conclusion

Available neural models of RF self-interference (SI) are typically architected with a strong orientation in domain knowledge of inband full-duplex systems. Limitations are then demonstrated by the specific model architecture, the variability of the SI channel and/or the nonlinearity in it. Our study

provides a structured dataset for these various difficulties in SI modeling. Moreover, we propose the parallel / adaptive Hammerstein neural network SI model to cope with the difficult configuration of variable SI channel and nonlinearity. It beats available neural network models, but polynomial modeling remains competitive in case of moderate nonlinearity.

REFERENCES

[1] M. Heino et al., "Recent advances in antenna design and interference cancellation algorithms for in-band full duplex relays," *IEEE Comm. Mag.*, vol. 53, no. 5, pp. 91–101, 2015.

[2] K.E. Kolodziej, B.T. Perry, and J.S. Herd, "In-band full-duplex technology: Techniques and systems survey," *IEEE Trans. Microwave Theory Techn.*, vol. 67, no. 7, pp. 3025–3041, 2019.

[3] B. Smida, A. Sabharwal, G. Fodor, G.C. Alexandropoulos, H.A. Suraweera, and C. Chae, "Full-duplex wireless for 6G: Progress brings new opportunities and challenges," *IEEE Jrnl. Selected Areas Commu.*, vol. 41, no. 9, pp. 2729–2750, 2023.

[4] A. Sabharwal, P. Schniter, D. Guo, D.W. Bliss, S. Rangarajan, and R. Wichman, "In-band full-duplex wireless: Challenges and opportunities," *IEEE Jrnl. Selected Areas in Communications*, vol. 32, no. 9, pp. 1637–1652, 2014.

[5] B. Smida, R. Wichman, K.E. Kolodziej, H.A. Suraweera, T. Riihonen, and A. Sabharwal, "In-band full-duplex: The physical layer," *Proc. of the IEEE*, vol. 112, no. 5, pp. 433–462, 2024.

[6] A.C.M. Austin, O. Afisiadis, and A. Burg, "Digital predistortion of hardware impairments for full-duplex transceivers," in *IEEE Global Conf. Sig. and Inf. Process. (GlobalSIP)*, 2017, pp. 878–882.

[7] F.H. Gregorio, G.J. González, J. Cousseau, T. Riihonen, and R. Wichman, "Predistortion for power amplifier linearization in full-duplex transceivers without extra RF chain," in *IEEE Intl. Conf. Acoustics, Speech and Signal Process. (ICASSP)*, 2017, pp. 6563–6567.

[8] A. Masmoudi and T. Le-Ngoc, "A maximum-likelihood channel estimator for self-interference cancelation in full-duplex systems," *IEEE Trans. Veh. Techn.*, vol. 65, no. 7, pp. 5122–5132, 2016.

[9] A. Masmoudi and T. Le-Ngoc, "Channel estimation and self-interference cancelation in full-duplex communication systems," *IEEE Tr. Veh. Techn.*, vol. 66, no. 1, pp. 321–334, 2017.

[10] H. Şenol, X. Li, and C. Tepedelenlioğlu, "Rapidly time-varying channel estimation for full-duplex amplify-and-forward one-way relay networks," *IEEE Trans. Signal Processing*, vol. 66, no. 11, pp. 3056–3069, 2018.

[11] X. Huang, A. Tuyen Le, and J.Y. Guo, "Joint analog and digital self-interference cancellation for full duplex transceiver with frequency-dependent I/Q imbalance," *IEEE Trans. Wireless Communications*, vol. 22, no. 4, pp. 2364–2378, 2023.

[12] J. Chu, Y. Tang, and Y. Zhou, "Digital domain self-interference cancellation based on modified variable step-size LMS algorithm," in *Intl. Conf. Communications, Information System and Computer Engineering (CISCE)*, 2023, pp. 9–14.

[13] A. Kiayani, M.Z. Waheed, L. Anttila, M. Abdelaziz, D. Korpi, V. Syrjälä, M. Kosunen, K. Stadius, J. Ryynänen, and M. Valkama, "Adaptive nonlinear RF cancellation for improved isolation in simultaneous transmit–receive systems," *IEEE Trans. Microwave Theory and Techniques*, vol. 66, no. 5, pp. 2299–2312, 2018.

[14] H. Vogt, G. Enzner, and A. Sezgin, "State-space adaptive nonlinear self-interference cancellation for full-duplex communication," *IEEE Trans. Sig. Process.*, vol. 67, no. 11, pp. 2810–2825, 2019.

[15] H. Esmaeili, A. Kariminezhad, and A. Sezgin, "Robust transceiver design for full-duplex decode-and-forward relay-assisted MIMO systems," in *Asilomar Conf. on Signals, Systems, and Computers*, 2020, pp. 1347–1352.

[16] M. Lari, "Matched-filter design to improve self-interference cancellation in full-duplex communication systems," *Wireless Networks*, vol. 29, no. 7, pp. 3137–3150, 2023.

[17] T. Le-Ngoc and Masmoudi A., *Full-Duplex Wireless Communications Systems: Self-Interference Cancellation*, Wireless Networks. Springer, 2017.

[18] C. Kong, G. Zhang, X. Liu, R. Li, J. Wang, and P. Wang, "Impact of pilot sequence on self-interference cancellation for full-duplex radios," in *IEEE Intl. Symp. Personal, Indoor and Mobile Radio Communications (PIMRC)*, 2019, pp. 1–6.

[19] V. Panse, T.K. Jain, P.K. Sharma, and A. Kothari, "Digital self-interference cancellation in the era of machine learning: A comprehensive review," *Phys. Comm.*, vol. 50, 2022.

[20] W. Zhang, J. Yin, D. Wu, G. Guo, and Z. Lai, "A self-interference cancellation method based on deep learning for beyond 5G full-duplex system," in *IEEE Intl. Conf. Signal Processing, Communications and Computing*, 2018, pp. 1–5.

[21] H. Guo, S. Wu, H. Wang, and M. Daneshmand, "DSIC: deep learning based self-interference cancellation for in-band full duplex wireless," in *IEEE Globecom*, 2019, pp. 1–6.

[22] A.T. Kristensen, A. Burg, and A. Balatsoukas-Stimming, "Advanced machine learning techniques for self-interference cancellation in full-duplex radios," in *Asilomar Conf. Signals, Systems, and Computers*, 2019, pp. 1149–1153.

[23] Y. Kurzo, A.T. Kristensen, A. Burg, and A. Balatsoukas-Stimming, "Hardware implementation of neural self-interference cancellation," *IEEE Jrnl. Emerging and Selected Topics in Circuits and Systems*, vol. 10, no. 2, pp. 204–216, 2020.

[24] M. Baek, J. Jung, H.M. Kim, H. Lee, and D. Choi, "Distortion element estimation technique based on deep learning for self-interference cancellation of full duplex communication system," in *IEEE Intl. Symp. Broadband Multimedia Systems and Broadcasting*, 2019, pp. 1–4.

[25] K. Muranov, M. Islam, B. Smida, and N. Devroye, "On deep learning assisted self-interference estimation in a full-duplex relay link," *IEEE Wireless Comm. Lett.*, vol. 10, no. 12, pp. 2762–2766, 2021.

[26] D.H. Kong, Y.-S. Kil, and S.-H. Kim, "Neural network aided digital self-interference cancellation for full-duplex communication over time-varying channels," *IEEE Trans. Vehicular Technology*, vol. 71, no. 6, pp. 6201–6213, 2022.

[27] M. Duarte, C. Dick, and A. Sabharwal, "Experiment-driven characterization of full-duplex wireless systems," *IEEE Trans. Wireless Comm.*, vol. 11, no. 12, pp. 4296–4307, 2012.

[28] A. Kiayani et al., "Adaptive nonlinear RF cancellation for improved isolation in simultaneous transmit–receive systems," *IEEE Trans. Microw. Theory Techn.*, vol. 66, no. 5, pp. 2299–2312, 2018.

[29] D. Korpi, L. Anttila, and M. Valkama, "Reference receiver based digital self-interference cancellation in MIMO full-duplex transceivers," in *IEEE Globecom*, 2014, pp. 1001–1007.

[30] E. Ahmed and A.M. Eltawil, "All-digital self-interference cancellation technique for full-duplex systems," *IEEE Trans. Wireless Communications*, vol. 14, no. 7, pp. 3519–3532, 2015.

[31] V. Erceg, L. Schumacher, P. Kyritsi, A. Molisch, D. Baum, Gorokhov A., et al., "TGn Channel Models (doc.: IEEE 802.11-03/940r4)," Tech. Rep., IEEE, May 2004.

[32] I. Qureshi and S. Asghar, "A systematic review of the IEEE-802.11 standard's enhancements and limitations," *Wireless Personal Comm.*, vol. 131, no. 4, pp. 2539–2572, 2023.

[33] M. Duarte et al., "Design and characterization of a full-duplex multiantenna system for WiFi networks," *IEEE Trans. on Vehicular Technology*, vol. 63, no. 3, pp. 1160–1177, 2013.

[34] A. Sethi, V. Tapio, and M. Juntti, "Self-interference channel for full duplex transceivers," in *IEEE Wireless Comm. Networking Conf.*, 2014, pp. 781–785.

[35] F. Chen, R. Morawski, and T. Le-Ngoc, "Self-interference channel characterization for wideband 2×2 MIMO full-duplex transceivers using dual-polarized antennas," *IEEE Trans. Antennas and Propagation*, vol. 66, no. 4, pp. 1967–1976, 2018.

[36] Y. S. Cho, J. Kim, W. Y. Yang, and C. G. Kang, *MIMO-OFDM Wireless Comm. with MATLAB*, John Wiley & Sons, 2010.

[37] J. Joung, C. K. Ho, K. Adachi, and S. Sun, "A survey on power-amplifier-centric techniques for spectrum- and energy-efficient wireless communications," *IEEE Comm. Surveys & Tutorials*, vol. 17, no. 1, pp. 315–333, 2014.

[38] J. Le Roux, S. Wisdom, H. Erdogan, and J. R. Hershey, "SDR – half-baked or well done?," in *IEEE Int. Conf. Acoust., Speech and Signal Process.*, 2019, pp. 626–630.

[39] J. Tellado, L.M.C. Hoo, and J.M. Cioffi, "Maximum-likelihood detection of nonlinearly distorted multicarrier symbols by iterative decoding," *IEEE Trans. Comm.*, vol. 51, no. 2, pp. 218–228, 2003.

[40] D.R. Morgan, Z. Ma, J. Kim, M.G. Zierdt, and J. Pastalan, "A generalized memory polynomial model for digital predistortion of RF power amplifiers," *IEEE Trans. Signal Processing*, vol. 54, no. 10, pp. 3852–3860, 2006.